FACTA UNIVERSITATIS
Series: **Mechanical Engineering**
https://doi.org/10.22190/FUME240125015V

Original scientific paper

HOMOGENISED PROPERTIES OF LATTICE METAL COMPOSITE CELL

Stefano Valvano

University of Derby, Institute of Innovation and Sustainable Engineering,
Lonsdale House, Derby, UK

Abstract. *In this paper, the mechanical analysis of an advanced Body Centred Cubic (BCC) lattice cell has been performed through a homogenisation procedure to obtain an equivalent set of mechanical properties. The mechanical analyses have been carried out with the use of ANSYS software and an original ANSYS Parametric Design Language (APDL) subroutine has been developed for the introduction of the double periodic boundary conditions. The Finite Element Method (FEM) is used for the mechanical model, and 3D elements with reduced integration has been employed to guarantee an accurate description of the lattice geometry. Different BCC cell configurations have been considered: standard metal BCC cell, metal BCC cell with waved struts, standard metal composite BCC cell. Depending on the configuration, the homogenised materials showed isotropic or orthotropic properties. For the evaluation of all the engineering constants, uniaxial traction test and in-plane shear test have been simulated along different loading directions. A parametric study has been conducted varying the struts diameter, the struts waviness and the thickness ratio of the composite struts. Finally, the homogenised materials have been tested through the mechanical analysis of sandwich panels with lattice core; a comparison between sandwich panels with homogenised core and sandwich panels with exact lattice cells has been carried out. The parametric study can be useful for the tailoring and optimisation analysis of an advanced component.*

Key words: *Lattice structure, FEM, Composite, Double periodicity, Homogenisation*

1. INTRODUCTION

In recent years, the ecological trends are motivating engineers to use fewer amounts of resources and to improve the design of lightweight structures, especially in transportation systems [1, 2]. The spread of Additive Manufacturing (AM) technologies is a clear example response to these trends. The AM production processes show a large parameter space,

Received: January 25, 2024 / Accepted March 21, 2024
Corresponding author: Stefano Valvano
University of Derby, Institute of Innovation and Sustainable Engineering, Lonsdale House, Quaker Way DE13HD, Derby, UK
E-mail: s.valvano@derby.ac.uk

which highly affects the components mechanical properties without increasing manufacturing costs due to the material usage reduction [3, 4]. Recently AM technologies are quickly spreading thanks to their promising process flexibility, the implementation of multi-materials and the capability to modify the function, structure shape and material properties, limited production costs with a weight reduction by up to 50% [5]. The parameter space complexity of AM production processes permits to derive periodic structures, advantageous for their mechanical properties relative to their weight or volume ratios [4]. In the family of highly periodic structures is possible to collocate the lattice cells and the porous cellular structures; this kind of structures offers a wide applications range and an interesting potential property tailoring [6-8]. The most influential AM process parameters should be identified and incorporated into the design and modelling process. In order to use the AM full potential, engineers need to develop and select convenient and appropriate design tools [4].

One of the design tools well known in the literature is the Representative Volume Element (RVE). The RVE can be defined as the smallest volume or cellular element statistically representative of the whole domain with a constitutive response error lower than 5% [9]. The RVE should be smaller compared to the whole structural domain, and in the meantime large to contain defects, in order to show a realistic mechanical response [10, 11]. Several studies have been proposed to determine the RVE size to keep computational costs low, [12, 13]. In the literature there are many important contributions on the topic of cellular materials, among others Gibson and Ashby [14], Masters and Evans [15], Christensen [16], and Wang and McDowell [17, 18] provided closed-form solutions to obtain the equivalent mechanical properties from the RVE definition. The main assumptions lay on the cellular components' description through the use of Euler-Bernoulli beams. This approach works well for relatively simple cellular architectures but presents limitations for complex cellular topology. Alternative approaches are based on energy equivalence methods [19, 20]. The analysis of the wave propagation in lattice structures and associated frequency characteristics has been investigated in many works [21, 22, 23, 24]. An equivalent continuum representation of periodic solids cellular structures can be investigated through homogenisation techniques. Multiscale methods have been developed using asymptotic expansion approaches [25, 26, 27]. Differently, Maewal [28] studied multiscale method with finite element approach, and in the works of McDevitt et al. [29, 30] the multiscale strategy has been proposed using the assumed strain method.

It is undoubted that FEM is the most used tool to analyse continuum micromechanics problems. The periodic homogenisation methods are based on the study of single repeating volume element. The asymptotic homogenisation [31] and the Macroscopic Degrees of Freedom [32] can be used with FEM codes. The Mechanics of Structural Genome [33] is a recent Finite Element based approaches for periodic homogenisation where the structure is analysed and divided in basic repeating elements as genome elements, and it is possible to pass from the macro to micro scale descriptions and vice versa using de-homogenisation and homogenisation techniques.

Several works have been made on the homogenisation of periodic cellular structures, among others the work of Seiler et al. [34] introduced the idea of waviness in 2D periodic grid cellular solids. A simplified homogenisation approach has been used for three-dimensional lattice cells in the work Alaimo et al. [35], Mantegna et al. [36] and Tumino et al. [37].

In this work, the mechanical analysis of an advanced Body Centred Cubic lattice cell has been performed through the derivation of the homogenisation procedure of periodic cellular structures in order to obtain an equivalent set of mechanical properties. An original ANSYS Parametric Design Language subroutine has been developed for the introduction of the double periodic boundary conditions. The originality of the work consists in the parametric study of different BCC cell configurations: standard metal BCC cell, metal BCC cell with waved struts, metal composite BCC cell. The approach used for the metal composite cell and the waviness struts present innovative idea for the tailoring of cellular solids, and it can be adapted for the study of multi-layered lattice cells or coated cellular structures. Results in terms of the homogenised materials are presented in tabular and figure forms.

2. Lattice Cell Structure

Sandwich panels are one of the most used light-weight structures [38], and many solutions have been proposed for the material selection and the architecture of sandwich cores [39]. The sandwich core concept, here adopted, is based on lattice structures, in particular the standard BCC cell (with straight struts) has been considered, moreover the author proposed the use of modified BCC cell with waved struts. In order to reduce the computational cost, the sandwich lattice core has been modelled through homogenised properties. In this section, the homogenisation process, based on the use of 3D FEM analysis performed in ANSYS environment, is described. The standard BCC cell structure has been directly drawn in Design Modeller environment, as shown in Fig. 1, a cylindrical strut section has been considered. The waved struts concept is built sweeping the strut circular section on an auxiliary diagonal plane (45°) following a three-point arch path, the single strut is copied mirroring it in the three Cartesian directions, see Fig. 2. For both the cell structures, the surface boundaries have been obtained through an intersection operation of the struts with a virtual bounding box. The strut material is an isotropic structural steel with the following properties: ρ = 7850 kg/m^3, E = 200 GPa, ν = 0.3 and G = 76.9231 GPa. The external bounding box (which defines the cells dimension) is a cube with edge length L = 10 mm.

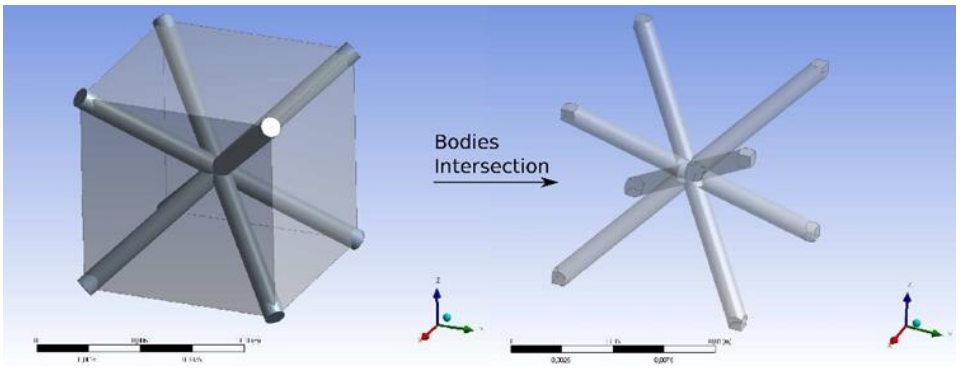

Fig. 1 BCC cell geometry definition, straight struts

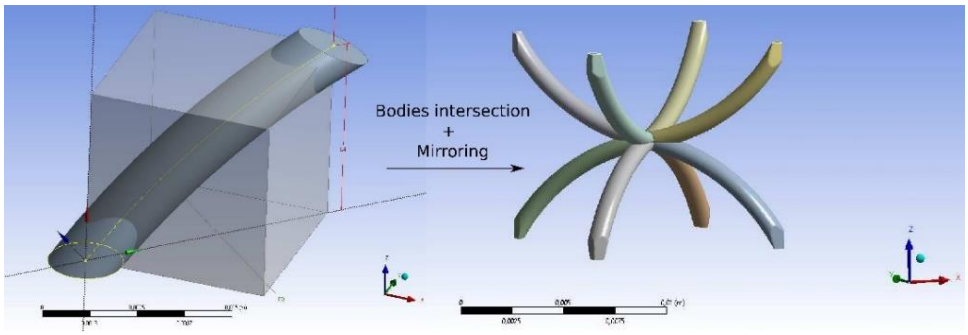

Fig. 2 BCC cell geometry definition, waved struts based on circumferential arch path

3. STRAIGHT STRUT

After the BCC cell geometry and the structural material definitions, the 3D meshing has been conducted in ANSYS using tetrahedral elements with an element dimension around a third of the strut radius, this ratio guarantees an acceptable convergence on the results. In order to apply the boundary conditions, it is important to define the outer boundary surfaces with respect to the direction of its normal. In Fig. 3, it is possible to see the four top surfaces (green colour) named z^+, the bottom surfaces (purple colour) named z^-, the left and the front ones (blue and black colours) called y^+ and x^-; y^- and x^+ are not reported in the figure for the sake of readability. The boundaries conditions are defined imposing a prescribed displacement on the FEM nodes lying on the boundary surfaces. In order to determine the Young modulus E, a traction (or compression) has been imposed to the z^+ surfaces through a prescribed displacement along the z direction, furthermore the reaction force could be obtained from the lower boundary surfaces z^- where the prescribed displacement is set to zero only for the z component. In order to make the present homogenisation campaign consistent, it is mandatory to ensure the compatibility of displacements along the faces of the representative volume element; in other words, the double periodic boundary conditions are applied to the surfaces with normal different with respect to the loading direction, as shown in Fig. 4.

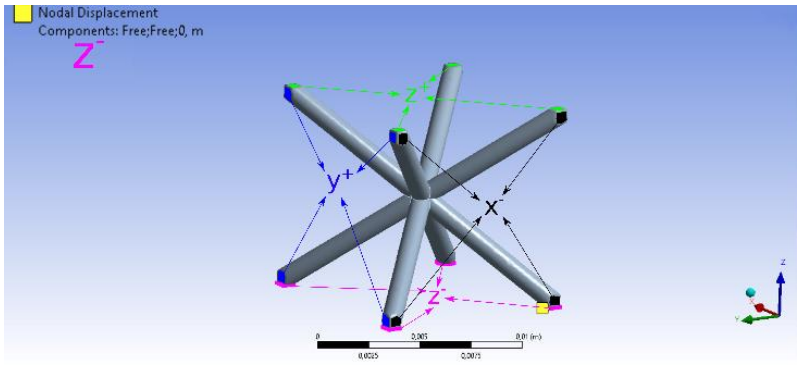

Fig. 3 BCC cell with straight struts, boundary definition

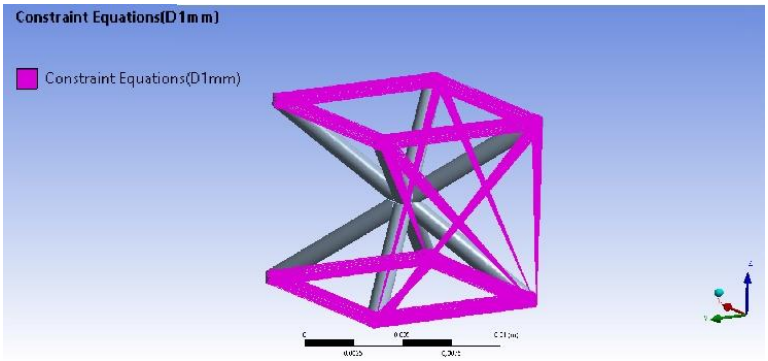

Fig. 4 BCC cell with straight struts, constraint equations applied

The periodicity concept implies that the representative volume element has the same deformation mode and there is no separation or overlap between adjacent volume elements [40, 41], the periodicity condition can be introduced as follows:

$$u_i = \bar{\epsilon}_{ik} x_k + u_i^* \tag{1}$$

where $\bar{\epsilon}_{ik}$ are the average strains and u_i^* is the unknown periodic part of the displacement components on the boundary surfaces. The displacements on a pair of opposite boundary surfaces can be derived as follows:

$$\begin{aligned} u_i^{j+} &= \bar{\epsilon}_{ik} x_k^{j+} + u_i^* \\ u_i^{j-} &= \bar{\epsilon}_{ik} x_k^{j-} + u_i^* \end{aligned} \tag{1}$$

where the index j stands for the normal direction of the upper (+) and lower (-) boundary surfaces. The difference between the displacement of the upper and lower boundary surfaces can be defined as:

$$u_i^{j+} - u_i^{j-} = \bar{\epsilon}_{ik}\left(x_k^{j+} - x_k^{j-}\right) = \bar{\epsilon}_{ik} \Delta x_k^j \tag{2}$$

For a cubic representative volume element and generally for a parallelepiped volume element, the term Δx_k^j can be considered constant; therefore, a generic periodic boundary condition can be defined as follows:

$$u_i^{j+}(x, y, z) - u_i^{j-}(x, y, z) = c_i^j \tag{3}$$

where the c_i^j constants represent the stretch or contraction terms of the representative volume element. It is possible to define the average stresses $\bar{\sigma}_{ij}$ and strains $\bar{\epsilon}_{ij}$ of the representative volume element as:

$$\bar{\epsilon}_{ij} = \frac{1}{V}\int_V \epsilon_{ij}\, dV \quad ; \quad \bar{\sigma}_{ij} = \frac{1}{V}\int_V \sigma_{ij}\, dV \tag{4}$$

where ϵ_{ij} and σ_{ij} are the local strains and stresses of the volume element V constituents. In order to apply the double periodicity in ANSYS environment, the author wrote an APDL routine: after checking the same position of two nodes placed on opposite boundary surfaces (one node on the x^+ and the other one on the x^-), for every pair of outer surface nodes a set of constraint equations is created, as follows:

$$\begin{aligned} u_i^+ - u_i^- &= \Delta_u \quad ; \quad \Delta_u = u_{ref}^+ - u_{ref}^- \\ v_i^+ - v_i^- &= \Delta_v \quad ; \quad \Delta_v = v_{ref}^+ - v_{ref}^- \\ w_i^+ - w_i^- &= \Delta_w \quad ; \quad \Delta_w = w_{ref}^+ - w_{ref}^- \end{aligned} \tag{5}$$

In Eq. 5 the basic constraint equations are expressed for a single direction, the mechanical displacements for each pair of i^{th} nodes could be linked considering a Δ term, which represents the stretch/dilatation property of the cell structure, calculated just choosing a reference pair of nodes. Applying the double periodicity condition, depending on the structure geometry, some nodes of the mesh could lay on two distinct boundary surfaces with two different normal; those shared nodes must be left free, without any constraint. The loading and boundary conditions applied are different in order to evaluate the Young modulus *E*, the Poisson coefficient *v* or the shear modulus *G*, therefore a resume of the used boundaries is listed in Table 1.

Table 1 BCC cell with straight struts, boundary conditions resume

Outer surfaces	x^+	x^-	y^+	y^-	z^+	z^-
E	*u=periodic* *v=periodic* *w=periodic*	*u=periodic* *v=periodic* *w=periodic*	*u=periodic* *v=periodic* *w=periodic*	*u=periodic* *v=periodic* *w=periodic*	*u=free* *v=free* *w=load*	*u=free* *v=free* *w=0*
v	*u=periodic* *v=periodic* *w=periodic*	*u=periodic* *v=periodic* *w=periodic*	*u=periodic* *v=periodic* *w=periodic*	*u=periodic* *v=periodic* *w=periodic*	*u=free* *v=free* *w=load*	*u=free* *v=free* *w=0*
G	*u=periodic* *v=periodic* *w=periodic*	*u=periodic* *v=periodic* *w=periodic*	*u=periodic* *v=periodic* *w=periodic*	*u=periodic* *v=periodic* *w=periodic*	*u= load* *v=free* *w=0*	*u=0* *v=free* *w=0*

A traction test campaign has been conducted in order to evaluate the Young modulus *E* and the Poisson coefficient *v*, different strut diameters has been considered, *D* = 1, 1.5, 2 mm. Calling the Hooke law: $\sigma = E\epsilon$, it is possible to obtain the Young Modulus *E* knowing the stress and the strain. The strain is immediately known because the traction is applied as a prescribed displacement on the top boundaries z^+. The equivalent stress can be calculated starting from the reaction force, obtained from the lower boundary surfaces z^- where the prescribed displacement is set to zero only for the *z* component, furthermore the equivalent stress can be calculated as:

$$\sigma_{equivalent}^{z} = \frac{\sum F_{reaction}^{z}}{A_{equivalent}} \tag{6}$$

where $A_{equivalent} = L^2$ and *L* is the maximum edge dimension of the full cube cell. The Poisson coefficient ν is defined as:

$$\nu = -\frac{\epsilon_{transverse}}{\epsilon_{loading}} \tag{7}$$

As mentioned before, $\epsilon_{loading}$ is known due to the prescribed loading displacement, differently $\epsilon_{transverse}$ should be calculated along the *x* or *y* direction, simply as:

$\epsilon_{xx}=(u_x^+-u_x^-)/L$ or $\epsilon_{yy}=(v_y^+-v_y^-)/L$. An example of a traction test results is given in Fig. 5 for a BCC cell with D = 1 mm strut diameter. In order to evaluate the shear modulus G a shear test campaign, for various strut diameters D = 1, 1.5, 2 mm, has been carried out. It is possible to obtain the shear modulus G knowing the stress and the strain and using the Hooke law: $\tau = G\epsilon$. As the previous case, the strain is known due to the prescribed displacement on the top boundaries z^+ and the equivalent stress is obtained from the reaction force as:

$$\tau_{equivalent}^{zx} = \frac{\sum F_{reaction}^{zx}}{A_{equivalent}} \tag{8}$$

where the loading direction can be x or y direction. Shear test results are given in Fig. 6 for a BCC cell with D = 2 mm strut diameter. Due to the isotropic geometric properties of the BCC cell and the isotropic properties of the considered strut material, it is worth noting that the homogenised properties will be of an isotropic material. Finally, in order to completely define the homogenised properties of the standard BCC cell, the equivalent density has been calculated as follows: $\rho = \rho_{steel}(V_{BCC}/V_{cube\ cell})$, where V_{BCC} is the volume of the considered BCC cell structure and $V_{cube\ cell}$ is the volume of the equivalent full cube cell. The homogenised isotropic properties of the standard BCC cell for different strut diameters are reported in Table 2.

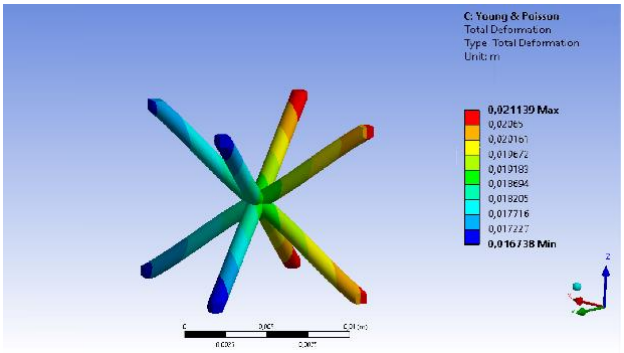

Fig. 5 Total displacement for BCC cell with thin diameter, traction test

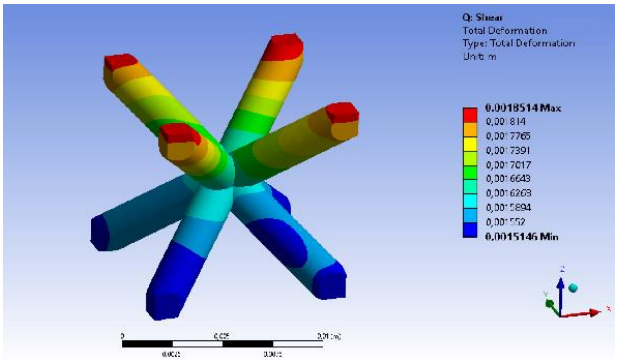

Fig. 6 Total displacement for BCC cell with thick diameter, shear test

Table 2 BCC cell with straight struts, homogenised properties for different strut diameters (D)

D [mm]	1	1.5	2
ρ [kg/m^3]	386.82	828.41	1396.99
E [MPa]	70.764	408.59	1473.7
ν [-]	0.492	0.479	0.46
G [MPa]	1263.8	2927.7	5384.3

In order to validate the present homogenisation approach, a static analysis of different sandwich panels with lattice core has been conducted. Two types of panels have been considered: a sandwich one with the skins made of structural steel and the lattice core based on standard BCC cells; a second panel with the same geometry and the same skins, but with a core layer based on the homogenised properties. The panels have simply-supported boundary conditions on all the lateral surfaces and a constant uniform pressure is applied on the top surface. First of all, a lattice core with 5 × 5 BCC cells has been considered; in Fig. 7 it is possible to note the displacement distribution on the top surface, the local effects of the struts are clearly visible. In Fig. 8 the displacement distribution on the bottom surface shows a global behaviour. The maximum displacement of the bottom surface is taken for comparison with the other plate model, the maximum bottom displacement for the sandwich with core made of 5 × 5 BCC cells is: −0.014638 mm.

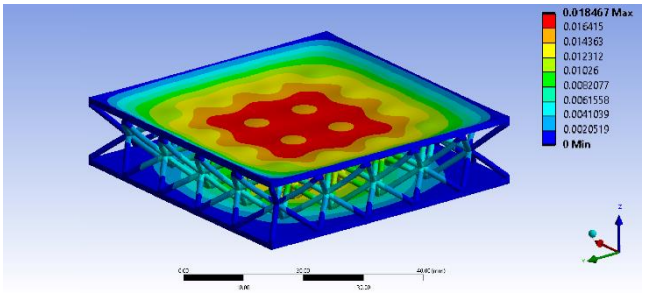

Fig. 7 Total displacement of the sandwich plate with lattice core made of 5×5 pattern BCC cells with straight struts, side and top view

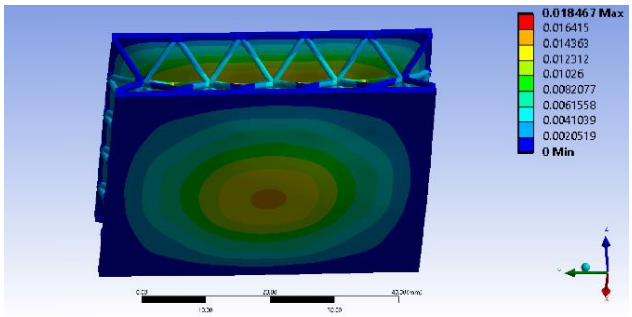

Fig. 8 Total displacement of the sandwich plate with lattice core made of 5×5 pattern BCC cells with straight struts, bottom view

Another sandwich configuration is taken into account, the same steel skins and a lattice core with 10 × 10 BCC cells, in Fig. 9 the undeformed panel geometry is depicted. The displacement of the loaded structure is represented in Fig. 10, it is clear that the top surface displacement shows a more global behaviour, differently with respect to the 5 ×5 pattern core. The maximum displacement of the bottom surface is taken for comparison with the homogenised plate model, the maximum bottom displacement for the sandwich with core made of 10 × 10 BCC cells is: −0.080943 mm.

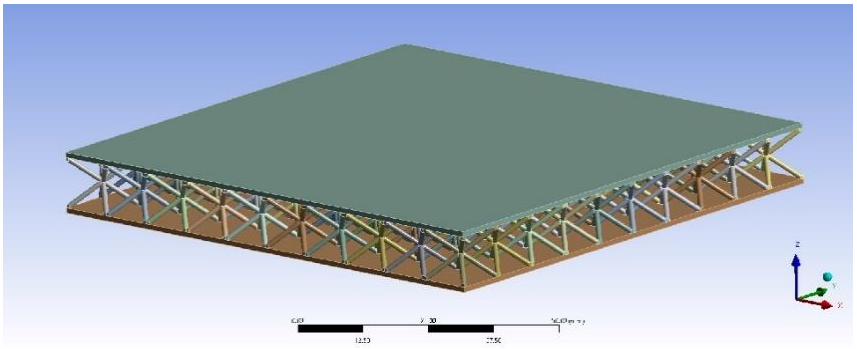

Fig. 9 Sandwich plate with lattice core made of 10 × 10 pattern BCC cells with straight struts

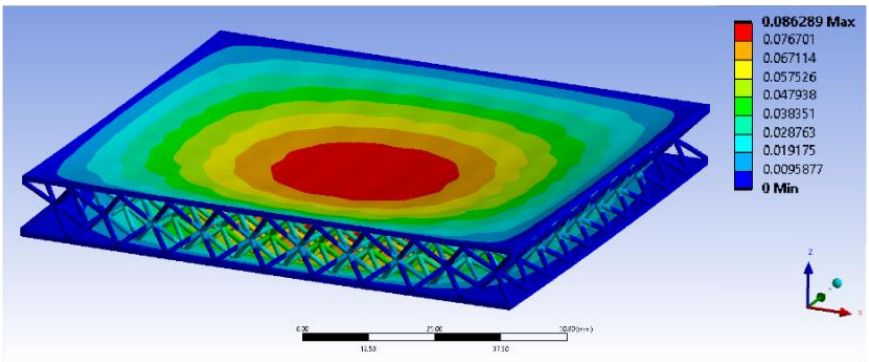

Fig. 10 Total displacement of the sandwich plate with lattice core made of 10 × 10 pattern BCC cells with straight struts

Finally, sandwich panels with homogenised core have been analysed, in Fig. 11 the 5 × 5 pattern core is represented, it has to be noticed that the local effects, due to the struts of the original core, on the top surface are missing. The maximum deflection of the bottom surface is equal to −0.013473 mm. In Fig. 12, the deformed sandwich structure with homogenised core is represented corresponding to 10×10 pattern cells. The displacement distribution of the top surface is similar to the original sandwich panel. The maximum deflection of the bottom surface is equal to −0.076095 mm.

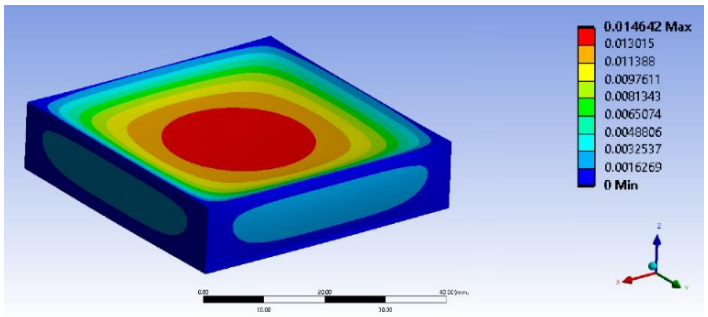

Fig. 11 Total displacement of the sandwich plate with homogenised core made of 5 × 5 BCC cells with straight struts

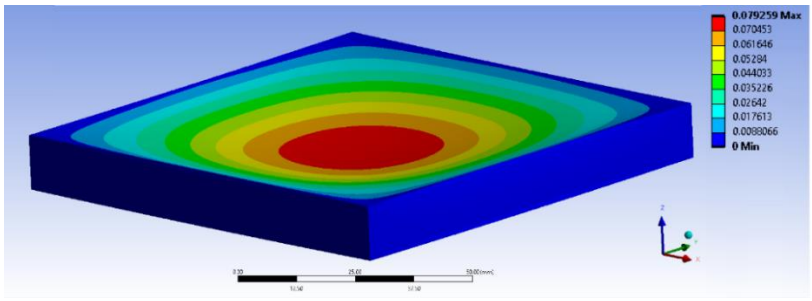

Fig. 12 Total displacement of the sandwich plate with homogenised core made of 10 × 10 BCC cells with straight struts

Comparing the maximum deflections of the original sandwich panel with 5 ×5 cell pattern core and that of the sandwich one with homogenised core, the homogenised model leads to an error of 7.96 %. Moreover, the same comparison for the 10×10 pattern core leads to an error of the homogenised model equal to 6 %. It is clear that, increasing the number of lattice cells in the core pattern, the structural response of the sandwich panel with original lattice core tends to be similar to the behaviour of the homogenised structure (the error decrease), where its core properties have been calculated with double periodicity condition. This ideally means an infinite number of cells in two directions.

4. WAVED STRUT

The homogenisation campaign continues with a modified BCC geometry, the author proposes here to introduce waviness into the strut path, in particular a three-point-arch path has been used for its definition. Different strut diameters, D = 1, 2 mm, and various path curvature, R = 10, 15, 20 mm, have been considered. The maximum cell dimension is kept fixed as the previous standard BCC cell with L = 10 mm. It is clear that the waviness concept introduces a reduction of the geometrical symmetry with respect to the standard BCC cell, consequently the waved BCC cell cannot keep the isotropic homogenised properties of the standard one, and it is well described by orthotropic homogenised

properties. The boundary surfaces are defined as the previous subsection and, for the sake of brevity, the discussion is not reported. In Table 3 a resume of the used boundary conditions is given in order to evaluate the orthotropic homogenised properties of the waved BCC cell: E_x, E_y, E_z, v_{xy}, v_{xz}, v_{yz}, G_{xy}, G_{xz}, G_{yz}.

Table 3 BCC cell with waved struts, boundary conditions resume

Outer surfaces	x^+	x^-	y^+	y^-	z^+	z^-
E_x	*u=load* *v=free* *w=free*	*u*=0 *v=free* *w=free*	*u=periodic* *v=periodic* *w=periodic*	*u=periodic* *v=periodic* *w=periodic*	*u=periodic* *v=periodic* *w=periodic*	*u=periodic* *v=periodic* *w=periodic*
E_z	*u=periodic* *v=periodic* *w=periodic*	*u=periodic* *v=periodic* *w=periodic*	*u=periodic* *v=periodic* *w=periodic*	*u=periodic* *v=periodic* *w=periodic*	*u=free* *v=free* *w=load*	*u=free* *v=free* *w*=0
v_{yx}	*u=load* *v=free* *w=free*	*u*=0 *v=free* *w=free*	*u=periodic* *v=periodic* *w=periodic*	*u=periodic* *v=periodic* *w=periodic*	*u=periodic* *v=periodic* *w=periodic*	*u=periodic* *v=periodic* *w=periodic*
v_{xz}	*u=periodic* *v=periodic* *w=periodic*	*u=periodic* *v=periodic* *w=periodic*	*u=periodic* *v=periodic* *w=periodic*	*u=periodic* *v=periodic* *w=periodic*	*u=free* *v=free* *w=load*	*u=free* *v=free* *w*=0
G_{xy}	*u*=0 *v=load* *w=free*	*u*=0 *v*=0 *w=free*	*u=periodic* *v=periodic* *w=periodic*	*u=periodic* *v=periodic* *w=periodic*	*u=periodic* *v=periodic* *w=periodic*	*u=periodic* *v=periodic* *w=periodic*
G_{xz}	*u*=0 *v=free* *w=load*	*u*=0 *v=free* *w*=0	*u=periodic* *v=periodic* *w=periodic*	*u=periodic* *v=periodic* *w=periodic*	*u=periodic* *v=periodic* *w=periodic*	*u=periodic* *v=periodic* *w=periodic*
G_{zx}	*u=periodic* *v=periodic* *w=periodic*	*u=periodic* *v=periodic* *w=periodic*	*u=periodic* *v=periodic* *w=periodic*	*u=periodic* *v=periodic* *w=periodic*	*u=load* *v=free* *w*=0	*u*=0 *v=free* *w*=0

The Poisson coefficients v_{ij} for orthotropic materials are defined as:

$$v_{ij} = -\frac{\epsilon_j}{\epsilon_i} \tag{9}$$

where ϵ_j is the strain in the transverse direction and ϵ_i is the strain in the axial loading direction. Considering the first test of the previous subsection, the traction test with the load applied along the *Z* direction, it is possible to obtain the Young modulus E_z and the Poisson coefficients $v_{zx} = v_{zy}$, in Fig. 13 the test is depicted in *Z* direction of a D = 1 mm, R = 10 mm waved BCC cell. The steps for the evaluation of the Young modulus and the Poisson coefficients are the same of the previous subsection case, for the sake of brevity the discussion is not here reported. Moreover, the Poisson coefficients rule for orthotropic materials permits to calculate v_{xz} and v_{yz} as follows:

$$\frac{v_{ij}}{E_i} = \frac{v_{ji}}{E_j} \tag{10}$$

The validity of this rule, applied to the waved BCC cell, has been verified by the author from the traction tests. Due to the geometric asymmetry of the waved BCC cell, another traction test is needed, in Fig. 14 the test in *X* direction of a D = 1 mm, R = 10 mm waved BCC cell is represented. Performing this test in *X* direction it possible to get the Young modulus E_x and the Poisson coefficient v_{xy}. Due to the geometric symmetry of the waved

BCC cell between the X and Y directions it is possible directly to assume that $E_y = E_x$ (for the sake of clarity, this assumption has been verified by the author).

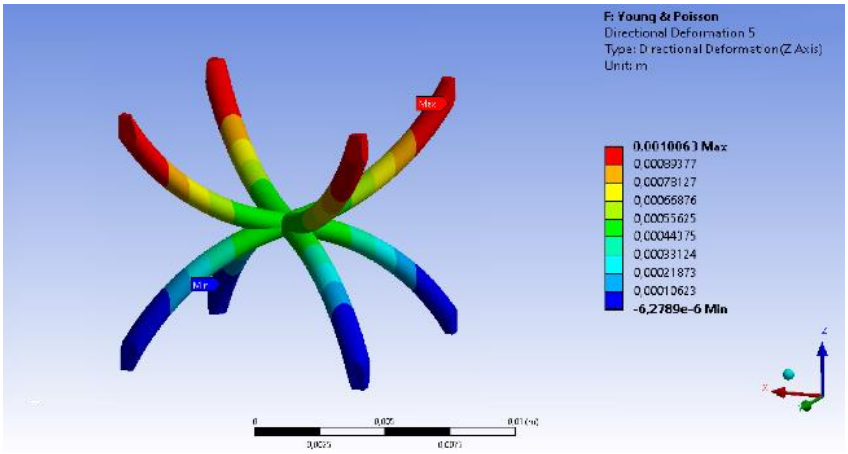

Fig. 13 Directional displacement of the waved cell (D = 1 mm, R = 10 mm) for the traction test, load applied in the Z direction

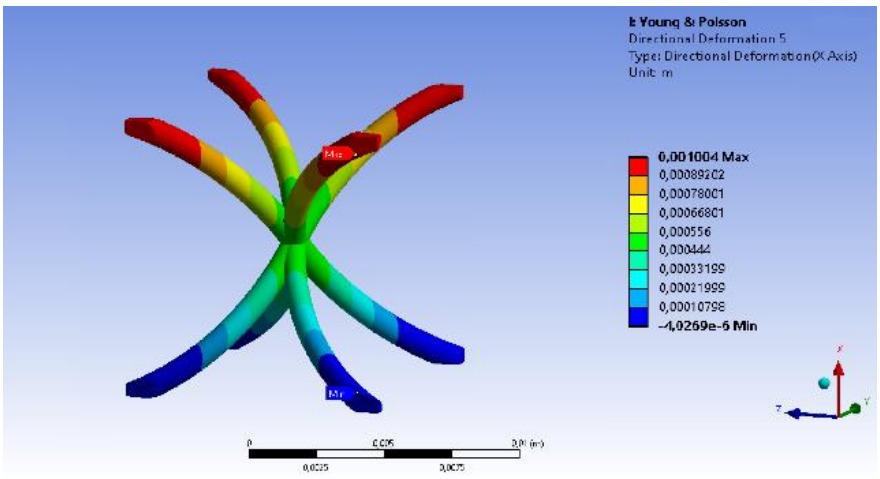

Fig. 14 Directional displacement of the waved cell (D = 1 mm, R = 10 mm) for the traction test, load applied in the X direction

In order to complete the homogenised properties definition, the shear moduli have to be defined. In Fig. 15 the shear test is represented (D = 2 mm, R = 20 mm), loading in X direction, it is possible to get the shear modulus G_{zx}. Differently from the previous standard BCC cell with straight struts, the geometric asymmetry of the waved BCC cell between the X and Z directions suggests verifying the shear response of the cell in Z direction. In Fig. 16 the shear test is depicted (D = 2 mm, R = 20 mm) in Z direction, due to the geometric asymmetry the author found that, for the waved BCC cell, $G_{zx} \neq G_{xz}$.

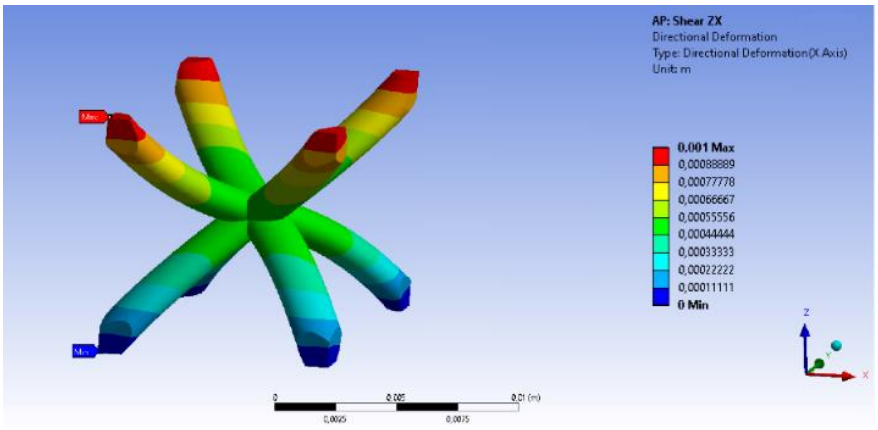

Fig. 15 Directional displacement of the waved cell (D = 2 mm, R = 20 mm) for the shear test, load applied in the X direction

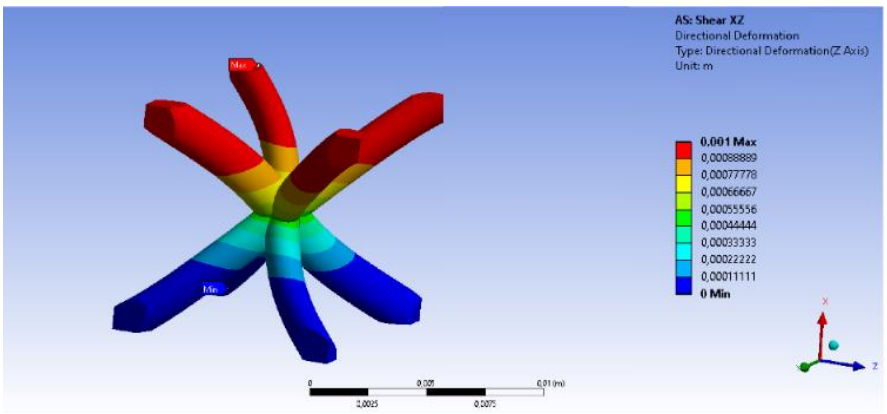

Fig. 16 Directional displacement of the waved cell (D = 2 mm, R = 20 mm) for the shear test, load applied in the Z direction

Considering that for classical elastic material formulation, the shear contribution is taken into account as follows:

$$\overline{\tau}_{ij} = \tau_{ij} + \tau_{ji} = G\frac{\partial u_j}{\partial i} + G\frac{\partial u_i}{\partial j} = G\left(\frac{\partial u_j}{\partial i} + \frac{\partial u_i}{\partial j}\right) \tag{11}$$

Rewriting Eq. 12 for the present waved BCC cell problem, it follows:

$$\begin{gathered}\overline{\tau}_{ij} = \tau_{ij} + \tau_{ji} = G_{ij}\frac{\partial u_j}{\partial i} + G_{ji}\frac{\partial u_i}{\partial j} \Rightarrow \\ \Rightarrow \overline{G}\left(\frac{\partial u_j}{\partial i} + \frac{\partial u_i}{\partial j}\right) = G_{ij}\frac{\partial u_j}{\partial i} + G_{ji}\frac{\partial u_i}{\partial j} \Rightarrow \\ \Rightarrow \overline{G} = \frac{G_{ij}\frac{\partial u_j}{\partial i} + G_{ji}\frac{\partial u_i}{\partial j}}{\left(\frac{\partial u_j}{\partial i} + \frac{\partial u_i}{\partial j}\right)}\end{gathered} \tag{12}$$

The homogenised properties for the shear moduli $\bar{G}_{xz} = \bar{G}_{yz}$ have been obtained as discussed in Eq. (13), differently the shear modulus G_{xy} is calculated from a single shear test, due to the symmetry between the X and Y directions. The homogenised orthotropic properties of the waved BCC cell for different strut diameters and different curvature radii are reported in Table 4.

Table 4 BCC cell with waved struts, homogenised properties for different strut diameters (D) and waviness radii (R)

D [mm]	1			2		
R [mm]	10	15	20	10	15	20
ρ [kg/m^3]	339.38	309.01	290.66	1201.8	1115.2	1057.2
E_x=E_y [MPa]	61.032	49.418	43.248	1379.9	1071.1	910.05
E_z [MPa]	71.474	39.767	30.325	1845.2	915.93	659.74
ν_{xy} [-]	0.5125	0.3564	0.2766	0.5408	0.3687	0.2802
$\nu_{xz} = \nu_{yz}$ [-]	0.4355	0.6150	0.7033	0.3432	0.5461	0.6501
G_{xy} [MPa]	710.59	693.50	709.68	4487.0	4018.1	3769.6
$G_{xz} = G_{yz}$ [MPa]	257.45	395.26	492.22	2605.3	3104.6	3260.9
$G_{zx} = G_{zy}$ [MPa]	318.50	450.32	537.33	2751.4	3225.6	3366.1
$\bar{G}_{xz} = \bar{G}_{yz}$ [MPa]	287.97	422.79	514.77	2678.3	3165.1	3313.5

In this subsection, the present 3D homogenisation approach for equivalent orthotropic material is validated considering an infinite sandwich panel using double-periodic boundary conditions. Two types of panels have been considered: a sandwich one with the skins made of structural steel and the lattice core based on three waved BCC cells along the thickness direction, see Fig. 17; a second panel with the same geometry and the same skins, but with a core layer based on the homogenised properties, see Fig. 18. The panels have double-periodic boundary conditions on all the lateral surfaces and a constant uniform displacement is applied on the top surface, the bottom surface has a fixed support along the loading direction Z, in other words $w(x,y,z=0) = 0$.

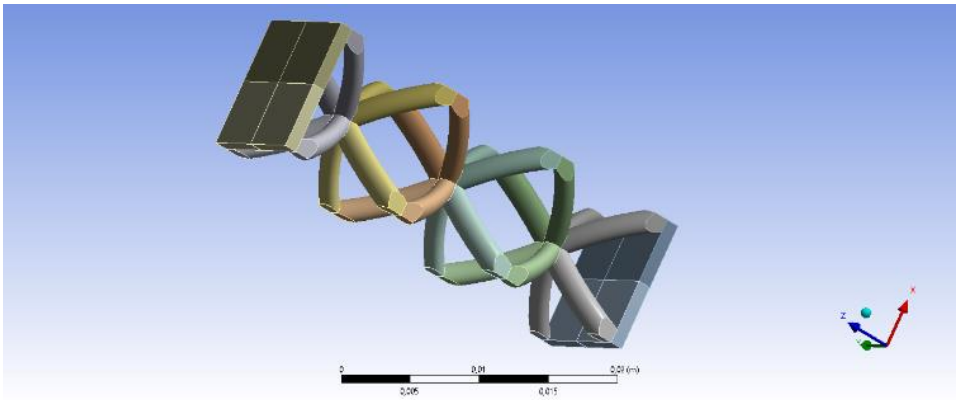

Fig. 17 Sandwich panel section made of structural steel skins and lattice core based on three waved BCC cells along the thickness direction

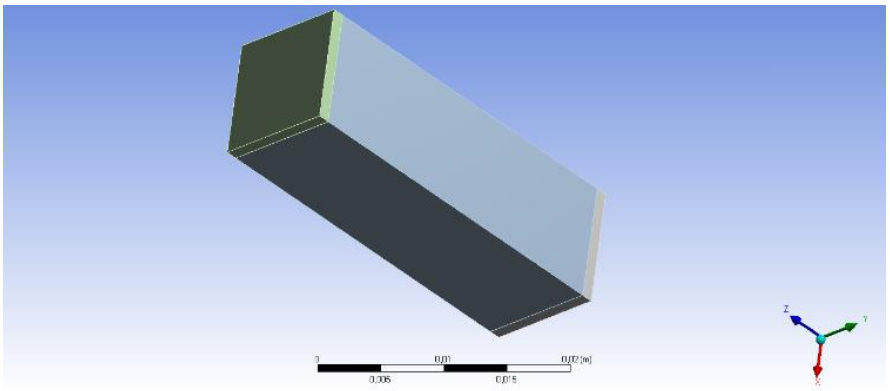

Fig. 18 Sandwich panel section made of structural steel skins and homogenised lattice core based on waved BCC cells

The sandwich panel with composite BCC cells shows a global structural response evaluated through the reaction force at the bottom surface, F_z = 10488 N. The sandwich panel with the homogenised core has a reaction force of F_z = 10635 N, it is clear that the homogenised model leads to an error of 1.5% on the global structural response.

Considering the stress distribution, it is well known that the lattice cell structures introduce local stress responses. The local stresses cannot be correctly detected by the homogenised models. However, the qualitative stress distribution on the top sandwich panel surface can be well described. The von Mises stress in the top surface central point of the sandwich panel with waved BCC cells is 1.341E9 Pa, for the homogenised model the Von Mises stress in the same evaluation point is 1.453E9 Pa. The local stress response is described with an error of 8.3% by the homogenised model. This local qualitative description is acceptable because is sufficiently far from the boundary conditions and from the lattice core where the lattice struts introduce stress concentration, see Fig. 19.

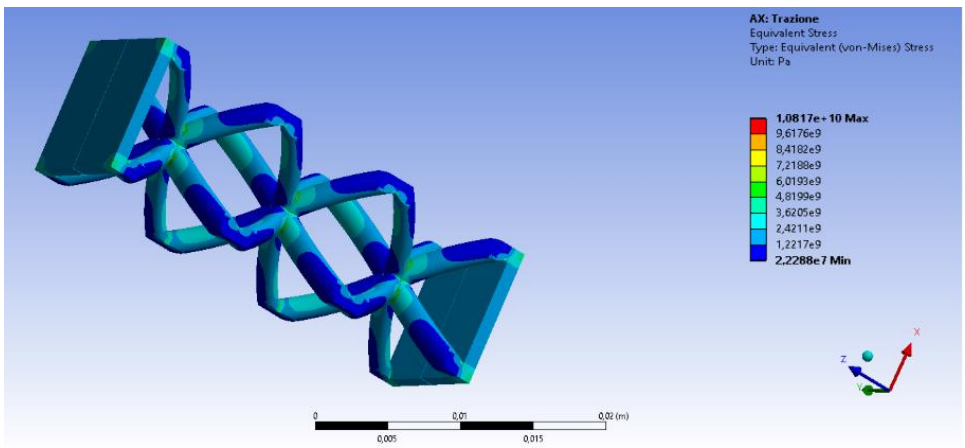

Fig. 19 Von Mises stress distribution along the sandwich panel section with structural steel skins and lattice core based on three waved BCC cells along the thickness direction

5. Composite Strut

The BCC geometry with straight strut is here considered. The author proposes to introduce metal matrix composite material with a concentric layup along the strut axis. The concentric multi-layered strut sequence is depicted in Fig. 20.

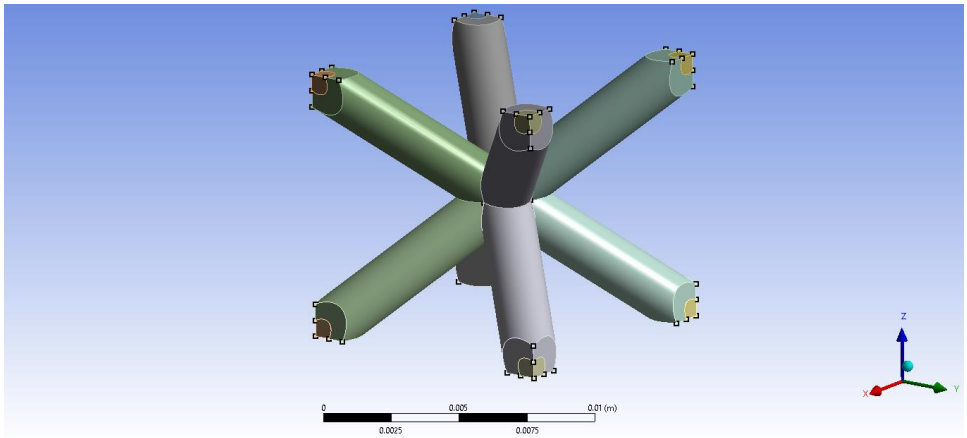

Fig. 20 Composite BCC cell with straight strut with a concentric layup along the strut axis

Different strut diameters D = 1, 2 mm as well as various thickness layup ratios $\bar{t} = t_{AlSiC} / t_{total} = 0.25, 0.5, 0.75$, have been considered. The maximum cell dimension is kept fixed as the previous standard BCC cell with L = 10 mm. The composite strut materials are made by an isotropic Aluminium and assumed isotropic metal matrix composite AlSiC with short fibres [42], the properties are resumed in Table 5, where V_f stands for volume fraction.

Table 5 Elastic properties for the composite strut cells, Aluminium and AlSiC [42] for different volume fractions

	ρ [kg/m^3]	E [GPa]	G [GPa]	v [-]
Aluminium	2610	76.8	28.8	0.333
AlSiC V_f 0.41 %	2860	138.9	56	0.239
AlSiC V_f 0.54 %	2940	183.9	74.4	0.235
AlSiC V_f 0.70 %	3020	224.6	91.2	0.231

The concentric material layup along the strut axis does not introduce any kind of asymmetry, the equivalent material has the same symmetry properties of the initial constituent ones, in other words the equivalent material can be assumed as isotropic. The boundary surfaces are defined as the first subsection and, for the sake of brevity, the discussion is not here reported. In Table 1 a resume of the used boundary conditions is given. The homogenised isotropic properties for the metal matrix composite BCC cell with concentric strut layup is given in Table 6.

Table 6 Homogenised properties of the metal matrix composite BCC cell for different materials thickness ratios $\bar{t}$ and different strut diameters D

			ρ [kg/m^3]	E [MPa]	G [MPa]	v [-]
D = 1		Aluminium	129.22	27.171	483.77	0.4914
		AlSiC V_f 0.41 %	141.59	48.115	879.44	0.4910
		AlSiC V_f 0.54 %	145.55	63.649	1164.6	0.4913
		AlSiC V_f 0.70 %	149.51	77.671	1422.7	0.4914
	$\bar{t}$ = 0.25	Aluminium + AlSiC Vf 0.41%	130.05	27.595	510.05	0.4917
		Aluminium + AlSiC Vf 0.54%	130.31	27.937	528.45	0.4918
		Aluminium + AlSiC Vf 0.70%	130.58	28.112	544.61	0.4920
	$\bar{t}$ = 0.5	Aluminium + AlSiC Vf 0.41%	132.46	29.567	586.67	0.4921
		Aluminium + AlSiC Vf 0.54%	133.50	30.954	658.37	0.4926
		Aluminium + AlSiC Vf 0.70%	134.54	32.116	722.75	0.4931
	$\bar{t}$ = 0.75	Aluminium + AlSiC Vf 0.41%	136.35	34.870	709.75	0.4923
		Aluminium + AlSiC Vf 0.54%	138.63	40.175	870.21	0.4928
		Aluminium + AlSiC Vf 0.70%	140.92	44.861	1015.0	0.4930
D = 2		Aluminium	465.74	565.79	2053.1	0.4611
		AlSiC V_f 0.41 %	510.35	983.23	3765.1	0.4603
		AlSiC V_f 0.54 %	524.63	1299.7	4988.0	0.4603
		AlSiC V_f 0.70 %	538.90	1584.9	6095.7	0.4603
	$\bar{t}$ = 0.25	Aluminium + AlSiC Vf 0.41%	468.99	584.50	2171.3	0.4612
		Aluminium + AlSiC Vf 0.54%	470.03	592.67	2248.2	0.4620
		Aluminium + AlSiC Vf 0.70%	471.07	598.55	2316.0	0.4626
	$\bar{t}$ = 0.5	Aluminium + AlSiC Vf 0.41%	478.12	634.50	2502.5	0.4627
		Aluminium + AlSiC Vf 0.54%	482.08	671.37	2805.7	0.4646
		Aluminium + AlSiC Vf 0.70%	486.04	700.88	3075.9	0.4661
	$\bar{t}$ = 0.75	Aluminium + AlSiC Vf 0.41%	492.21	741.44	3029.9	0.4633
		Aluminium + AlSiC Vf 0.54%	500.68	857.57	3710.5	0.4652
		Aluminium + AlSiC Vf 0.70%	509.15	957.79	4322.8	0.4665

Finally, the present 3D homogenisation approach for composite lattice structure is validated considering an infinite sandwich panel using double-periodic boundary conditions. Two types of panels have been considered: a sandwich one with the skins made of Aluminium and the lattice core based on three composite BCC cells, along the thickness

direction, made of Aluminium and AlSiC with thickness layup ratios $\bar{t} = 0.5$, see Fig. 21; a second panel with the same geometry and the same skins, but with a core layer based on the homogenised properties, see Fig. 22. The panels have the same boundary conditions of the previous subsection: double-periodic boundary conditions on all the lateral surfaces and a constant uniform displacement is applied on the top surface, the bottom surface has a fixed support along the loading direction Z, in other words $w(x,y,z=0) = 0$.

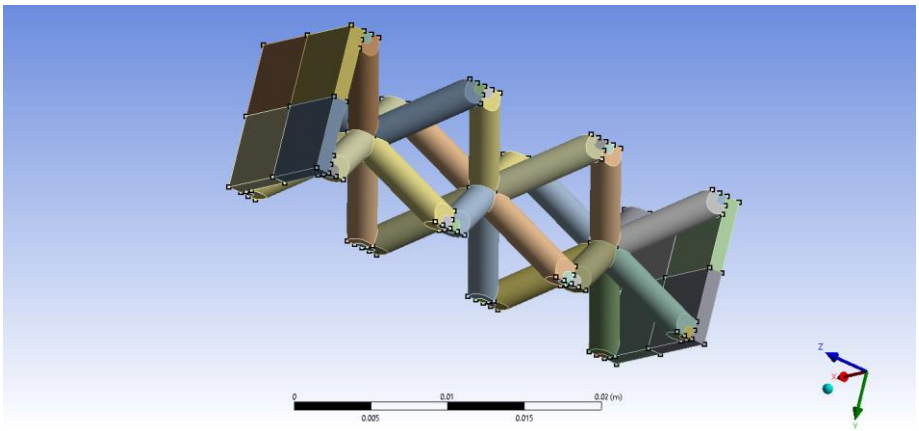

Fig. 21 Sandwich panel section assembled with Aluminium skins and lattice core based on three composite BCC cells, along the thickness direction, made of Aluminium and AlSiC with thickness layup ratios $\bar{t} = 0.5$

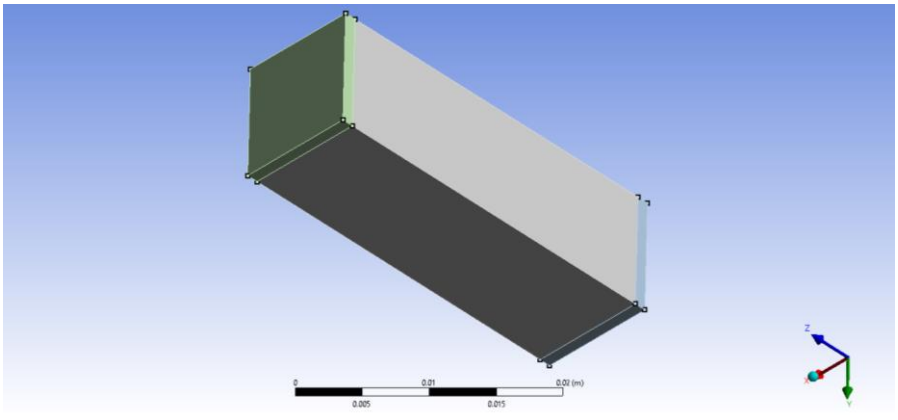

Fig. 22 Sandwich panel section assembled with Aluminium skins and homogenised lattice core based on three composite BCC cells made of Aluminium and AlSiC

The sandwich panel with composite BCC cells shows a global structural response evaluated through the reaction force at the bottom surface, $F_z = 7476.5$ N. The sandwich panel with the homogenised core has a reaction force of $F_z = 7392.3$ N, it is clear that the homogenised model leads to an error of 1.1% on the global structural response.

As the previous structural example, the local stresses cannot correctly be detected by the homogenised models. However, the qualitative stress distribution on the top sandwich panel surface can be well described. The Von Mises stress in the top surface central point of the sandwich panel with waved BCC cells is 8.941E8 Pa, for the homogenised model the Von Mises stress in the same evaluation point is 8.328E8 Pa. The local stress response is described with an error of 6.8% by the homogenised model. For the sake of completeness, the Von Mises stress distribution of the top surface of the sandwich panel with composite BCC cells is depicted in Fig. 23, the same stress distribution of the homogenised model is reported in Fig. 24.

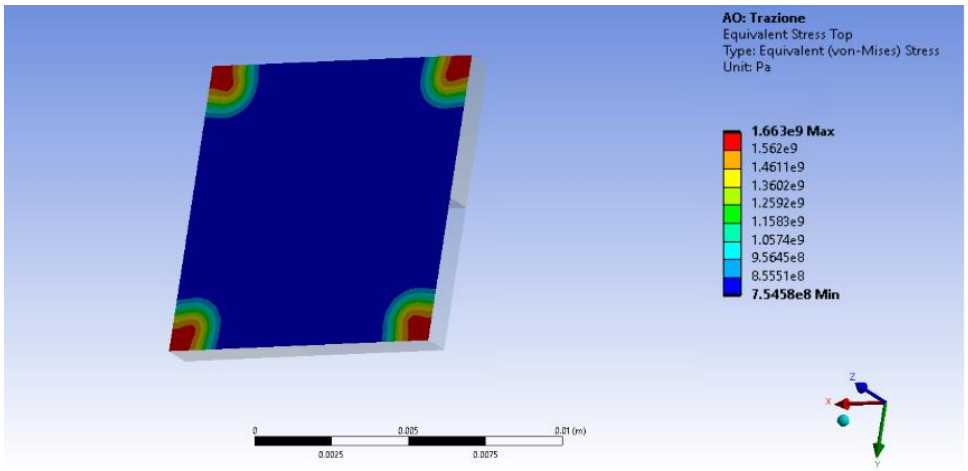

Fig. 23 Von Mises stress distribution on the top surface of the sandwich panel with composite BCC cells

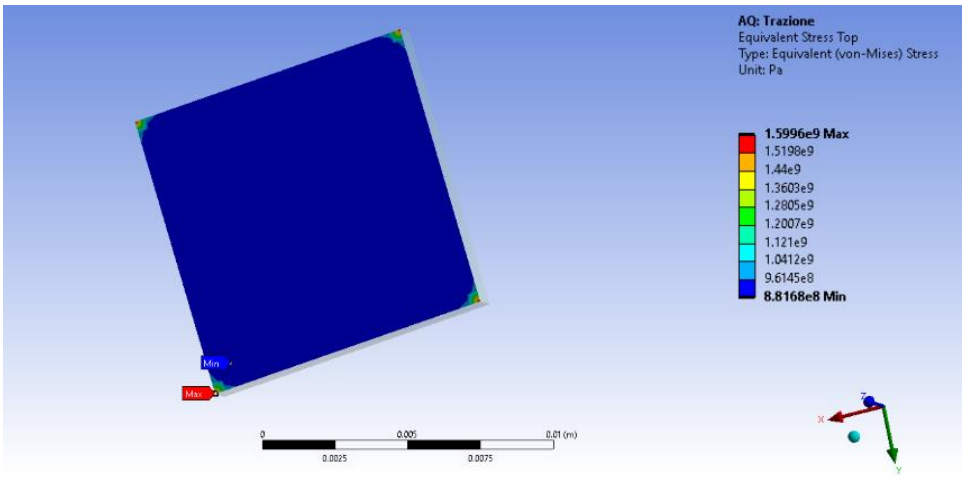

Fig. 24 Von Mises stress distribution on the top surface of the sandwich panel with homogenised core based on composite BCC cells

6. CONCLUSIONS

In this work, the mechanical analysis of an advanced Body Centred Cubic lattice cell has been performed through the derivation of the homogenisation procedure of periodic cellular structures in order to obtain an equivalent set of mechanical properties. An original ANSYS Parametric Design Language subroutine has been developed for the introduction of the double periodic boundary conditions. The originality of the work consists in the study of different BCC cell configurations: standard metal BCC cell, metal BCC cell with waved struts, metal composite BCC cell. The approach used for the metal composite cell and the waviness struts present innovative idea for the tailoring of cellular solids, and it can be adapted for the study of multi-layered lattice cells or coated cellular structures.

A parametric study has been conducted varying the struts diameter, the struts waviness and the thickness ratio of the composite struts. The following conclusions can be drawn:

- The BCC geometry configuration permits to obtain a structure with an equivalent shear modulus G greater with respect to the Young modulus E.
- Increasing the struts diameter, it is possible to increase both the shear and Young moduli, and at the same time reducing the Poisson ratio v value.
- The strut waviness introduces the concept of orthotropic properties for the description of the equivalent Young and shear moduli and the Poisson ratios.
- The increase of the waviness radius permits to reduce the Young moduli, the Poisson ratios and the G_{xy} shear modulus; at the same time the shear moduli $\bar{G}_{xz}$ and $\bar{G}_{yz}$ are increasing as the waviness radius.
- The composite strut permits to add an input to the tailoring of the lattice cell equivalent material properties. Increasing the thickness ratio $\bar{t}$, it is possible to get bigger Young and shear moduli and Poisson ratio.

The parametric studies can be useful for the tailoring and optimisation analysis of an advanced component. Finally, the homogenised materials have been tested through the mechanical analysis of sandwich panels with lattice core; a successful comparison between sandwich panels with homogenised core and sandwich panels with exact lattice cells has been carried out.

REFERENCES

1. Blakey-Milner, B., Gradl, P., Snedden, G., Brooks, M., Pitot, J., Lopez, E., Leary, M., Berto, F., Du Plessis, A., 2021, *Metal additive manufacturing in aerospace: A review*, Materials & Design, 209, 10008.
2. Rama, G., Marinkovic, D., Zehn, M., 2018, *High performance 3-node shell element for linear and geometrically nonlinear analysis of composite laminates*, Composites Part B: Engineering, 151, pp. 118-126.
3. Zhu, J.H., Zhou, H., Wang, C., Zhou, L., Yuan, S., Zhang, W., 2021, *A review of topology optimization for additive manufacturing: status and challenges*, Chinese Journal of Aeronautics, 34, pp. 91-110.
4. Plocher, J., Panesar, A., 2019, *Review on design and structural optimisation in additive manufacturing: Towards next-generation lightweight structures*, Materials & Design, 183, 108164.
5. Aboulkhair, N.T., Everitt, N.M., Ashcroft, I., Tuck, C., 2014, *Reducing porosity in AlSi10Mg parts processed by selective laser melting*, Additive Manufacturing, 1, pp. 77-86.
6. Chen, L.Y., Liang, S.X., Liu, Y., Zhang, L.C., 2021, *Additive manufacturing of metallic lattice structures: Unconstrained design, accurate fabrication, fascinated performances, and challenges*, Materials Science and Engineering: R: Reports, 146, 100648.
7. Du Plessis, A., Broeckhoven, C., Yadroitsava, I., Yadroitsev, I., Hands, C.H., Kunju, R., Bhate, D., 2019, *Beautiful and functional: a review of biomimetic design in additive manufacturing*, Additive Manufacturing, 27, pp. 408-427.

8. Sohrabian, M., Vaseghi, M., Khaleghi, H., Dehrooyeh, S., Kohan, M.S.A., 2021, *Structural investigation of delicate-geometry fused deposition modelingn additive manufacturing scaffolds: experiment and analytics*, Journal of Materials Engineering and Performance, 30(9), pp. 6529-6541.
9. Drugan, W.J., Willis, J.R., 1996, *A micromechanics-based nonlocal constitutive equation and estimates of representative volume element size for elastic composites*, Journal of the Mechanics and Physics of Solids, 44(4), pp. 497-524.
10. Hashin, Z., 1983, *Analysis of composite materials-A survey*, Journal of Applied Mechanics, 50(3), pp. 481-505.
11. Gitman, I.M., Askes, H., Sluys, L.J., 2007, *Representative volume: Existence and size determination*, Engineering Fracture Mechanics, 74(16), pp. 2518-2534.
12. Kanit, T., Forest, S., Galliet, I., Mounoury, V., Jeulin, D., 2003, *Determination of the size of the representative volume element for random composites: statistical and numerical approach*, International Journal of Solids and Structures, 40(13-14), pp. 3647-3679.
13. Borbely, A., Biermann, H., Hartmann, O., 2001, *FE investigation of the effect of particle distribution on the uniaxial stress-strain behaviour of particulate reinforced metal-matrix composites*, Materials Science and Egineering: A, 313(1-2), pp. 34-45.
14. Gibson, L.J., 2003, *Cellular solids*, Mrs Bulletin, 28(4), pp. 270-274.
15. Masters, I.G., Evans, K.E., 1996, *Models for the elastic deformation of honeycombs*, Composite Structures, 35(4), pp. 403-422.
16. Christensen, R.M., 2000, *Mechanics of cellular and other low-density materials*, International Journal of Solids and Structures, 37(1-2), pp. 93-104.
17. Wang, A.J., McDowell, D.L., 2004, *In-plane stiffness and yield strength of periodic metal honeycombs*, Journal of Engineering Materials and Technology, 126(2), pp. 137-156.
18. Wang, A.J., McDowell, D.L., 2005, *Yield surfaces of various periodic metal honeycombs at intermediate relative density*, International Journal of Plasticity, 21(2), pp. 285-320.
19. Kumar, R.S., McDowell, D.L., 2004, *Generalized continuum modelling of 2-D periodic cellular solids*, International Journal of Solids and Structures, 41(26), pp. 7399-7422.
20. Burgardt, B., Cartraud, P., 1999, *Continuum modelling of beamlike lattice trusses using averaging methods*, Computers & Structures, 73(1-5), pp. 267-279.
21. Phani, A.S., Woodhouse, J., Fleck, N.A., 2006, *Wave propagation in two-dimensional periodic lattices*, The Journal of the Acoustical Society of America, 119(4), pp. 1995-2005.
22. Martinsson, P.G., Movchan, A.B., 2003, *Vibrations of lattice structures and phononic band gaps*, Quarterly Journal of Mechanics and Applied Mathematics, 56(1), pp. 45-64.
23. Sigmund, O. Søndergaard Jensen, J., 2003, *Systematic design of phononic band-gap materials and structures by topology optimization*, Philosophical Transactions of the Royal Society of London, Series A: Mathematical, Physical and Engineering Sciences, 361(1806), pp. 1001-1019.
24. Hussein, M.I., Hulbert, G.M., Scott, R.A., 2003, *Band-gap engineering of elastic waveguides using periodic materials*, In ASME International Mechanical Engineering Congress and Exposition, 37122, pp. 799-807.
25. Fish, J., Chen, W., 2001, *Higher-order homogenization of initial/boundary-value problem*, Journal of Engineering Mechanics, 127(12), pp. 1223-1230.
26. Fish, J., Chen, W., Nagai, G., 2002, *Non-local dispersive model for wave propagation in heterogeneous media: one-dimensional case*, International Journal for Numerical Methods in Engineering, 54(3), pp. 331-346.
27. Fish, J., Chen, W., Nagai, G., 2002, *Non-local dispersive model for wave propagation in heterogeneous media: multi-dimensional case*, International Journal for Numerical Methods in Engineering, 54(3), pp. 347-363.
28. Maewal, A., 1986, *Construction of models of dispersive elastodynamic behaviour of periodic composites: a computational approach*, Computer Methods in Applied Mechanics and Engineering, 57(2), pp. 191-205.
29. McDevitt, T.W., Hulbert, G.M., Kikuchi, N., 2001, *An assumed strain method for the dispersive global-local modelling of periodic structures*, Computers Methods in Applied Mechanics and Engineering, 190(48), pp. 6425-6440.
30. McDevitt, T.W., Hulbert, G.M., Kikuchi, N., 1999, *Plane harmonic wave propagation in three-dimensional composite media*, Finite Elements in Analysis and Design, 33(4), pp. 263-282.
31. Suquet, P., 1987, *Elements of homogenization for inelastic solid mechanics*, Homogenization Techniques for Composite Media, 105, pp. 193-278.
32. Michel, J.C., Moulinec, H., Suquet, P., 1999, *Effective properties of composite materials with periodic microstructure: a computational approach*, Computer Methods in Applied Mechanics and Engineering, 172(1-4), pp. 109-143.
33. Yu, W., Tang, T., 2007, *Variational asymptotic method for unit cell homogenization of periodically heterogeneous materials*, International Journal of Solids and Structures, 44(11-12), pp. 3738-3755.
34. Seiler, P.E., Li, K., Deshpande, V.S., Fleck, N.A., 2021, *The influence of strut waviness on the tensile response of lattice materials*, Journal of Applied Mechanics, 88(3), 031011.

35. Alaimo, A., Marino, F., Valvano, S., 2021, *BCC lattice cell structural characterization*, Reports in Mechanical Engineering, 2(1), pp. 77-85.
36. Mantegna, G., Vindigni, C.R., Valvano, S., Esposito, A., Tumino, D., Alaimo, A., Orlando, C., 2023, *Representative volume element homogenisation approach to characterise additively manufactured porous metals*, Mechanics of Advanced Materials and Structures, 30(5), pp. 1073-1082.
37. Tumino, D., Alaimo, A., Mantegna, G., Orlando, C., Valvano, S., 2023, *Mechanical properties of BCC lattice cells with waved struts*, International Journal on Interactive Design and Manufacturing, https://doi.org/10.1007/s12008-023-01359-9.
38. Ha. G.X., Zehn, M.W., Marinkovic, D., Fragassa, C., 2019, *Dealing with nap-core sandwich composites: How to predict the effect of symmetry*, Materials, 12(6), 874.
39. Ha, G.X., Marinkovic, D., Zehn, M.W., 2019, *Parametric investigations of mechanical properties of nap-core sandwich composites*, Composites Part B: Engineering, 161, pp. 427-438.
40. Suquet, P., 1987, *Elements of homogenization theory for inelastic solid mechanics*, In: Sanchez-Palencia, E., Zaoui, A. (Eds.), Homogenization Techniques for Composite Media. Springer-Verlag, Berlin, pp. 194-275.
41. Xia, Z., Zhang, Y., Ellyin, F., 2003, *A unified periodical boundary conditions for representative volume elements of composites and applications*, International Journal of Solids and Structures, 40(8), pp. 1907-1921.
42. Kumar, S.S., Bai, V.S., Rajkumar, K.V., Sharma, G.K., Jayakumar, T., Rajasekharan, T., 2009, *Elastic modulus of Al-Si/SiC metal matrix composites as a function of volume fraction*, Journal of Physics D: Applied Physics, 42(17), 175504.